ELSEVIER

Contents lists available at ScienceDirect

Applied Surface Science Advances

journal homepage: www.elsevier.com/locate/apsadv



Effect of bubble nucleating agents derived from biochar on the foaming mechanism of poly lactic acid foams



Hai Haham a,b,*, Andrew Riscoeb, Curtis W. Frankb, Sarah L. Billingtona

- ^a Department of Civil & Environmental Engineering, Stanford University, 473 Via Ortega, Stanford, CA 94305-4020, United States
- b Department of Chemical Engineering, Stanford University, 433 Via Ortega, Stanford, CA 94305-4020, United States

ARTICLE INFO

Keywords: Surface chemistry Porous materials Biodegradable polymers Biochar PLA

ABSTRACT

Improvement and new technologies for effective poly (lactic acid) (PLA) foaming are still in developing. This study examines the ability of biochar (BC) to assist in PLA foaming through a supercritical CO₂ batch process. To determine suitable foaming parameters, process optimization was conducted on neat PLA films. BC particles derived from three different sources – sludge (SLG), pistachio shells (PST) and green waste (GW) were ground, and ball milled to a microscale and then blended with PLA. The PLA/BC blends were extruded into films and then batch foamed. The effect of BC was found to be concentration and source dependent. At 0.25 wt%, BC particles were found to be effective nucleating agents showing an increase up to four orders of magnitude in cell density and 10-fold reduction in the mean pore size compared to the neat PLA foams. An increase in BC content to 0.5 and 1 wt% induced particle aggregation, which resulted in non-homogenous foam densities. BC particles derived from SLG were the most effective nucleating agents due to their narrow size distribution, improved dispersibility and mesoporous surface. This work shows that BC can act as an effective bio-derived nucleating agent for PLA.

1. Introduction

Biodegradable polymers have become green alternatives to conventional plastics derived from non-renewable fossil fuels [1]. Poly(lactic acid) (PLA) is one of the main biodegradable polymers in the current emerging bioplastics market. PLA belongs to a family of aliphatic polyesters manufactured from renewable raw materials and it is considered biodegradable and compostable [2,3]. Due to its competitive processing costs and comparable mechanical properties, PLA is considered to be a promising replacement for polystyrene (PS) foam products for packaging [4], cushioning, construction, thermal and sound insulation [5]. Currently, the production of low-density PLA foams with a uniform cell morphology is still challenging due to its low melt strength and its thermal instability [6]. PLA is susceptible to thermal [7], oxidative [8] and hydrolytic degradation [9], which may occur during processing. All these degradation processes result in decreases of molecular weight and corresponding worsening of the rheological properties, which should be avoided for foaming, when high levels of extensional viscosity are required.

Foaming polymers using supercritical CO_2 has attracted considerable research attention as an environmental-friendly processing technique for fabrication of foams [5,10,11]. CO_2 is characterized by low flammability, toxicity and cost, which makes it attractive as blowing agent. In addition, CO_2 is easily removable from processed polymers,

In a supercritical foaming process, gas under supercritical conditions diffuses into the polymer, followed by a rapid change in temperature or pressure. This change in process conditions leads to a thermodynamic disequilibrium that induces a nucleation of the gaseous phase in cells. Once nuclei are formed in the polymer melt, they start to grow in order to reach a critical radius that allows them to sustain the pressure of the surrounding polymer melt. The change in the cell radius depends on the pressure drop rate, the viscosity of the polymer melt and the diffusivity of the CO_2 in the polymer [13]. In an optimal system, the viscosity of the polymer melt should be maintained low during nucleation and high during the late stage of foaming in order to stabilize the foam structure [14].

Many researchers have studied the contribution of nano and microsized additive fillers on PLA foams [15–17]. Well-dispersed fillers at an appropriate concentration can serve as preferential nucleation sites with a lower energy barrier for nucleation, thus facilitating the cell nucleation process. In addition, dispersed particles can simultaneously enhance the melt strength of the polymer matrix, thereby stabilizing nucleated cells by minimizing cell coalescence [18]. Consequently, a larger number of

E-mail address: haih@stanford.edu (H. Haham).

and thus may be used for "solvent-free" incorporation of additives [12]. CO_2 becomes a supercritical fluid when both pressure and temperature exceed a critical point at which CO_2 holds a combined gas-like viscosity and liquid-like density, making it an excellent solvent for foaming applications.

^{*} Corresponding author.

nucleated cells will last longer during cell growth, and the final expansion ratio of the foam products will also be promoted. For example, incorporation of organic nanoclay in PLA led to a five-fold increase in the polymer foam cell density in a batch foaming process [5]. Similarly, introduction of cellulose nanofibrils into the PLA matrix increased the cell density by two orders of magnitude and reduced the mean cell size of the foam from 50 to 10 μ m [13].

Nano and micro fillers such as cellulose nanofibrils or nanoclay are characterized with hydrophilic surface and therefore tend to aggregate in hydrophobic polymer matrices, as PLA^{17,18}. The literature offers various strategies to address the limited dispersibility of these bio-fillers in various polymer matrices which includes different processes, additive addition, and surface modifications ³⁶. These strategies are often expensive and difficult to implement especially in large scale productions. Biochar (BC), a bio-derived charcoal-like substance made by pyrolyzing organic material from organic waste, is relatively hydrophobic and presumably can present better compatibility to PLA, in comparison to other hydrophilic bioderived fillers.

This work presents the development of PLA/BC foams using a supercritical CO_2 batch foaming process. BC nano- and microparticles derived from sludge (SLG), pistachio (PST) and green waste (GW) were ground, sieved, ball-milled and compounded with PLA in different ratios through a thermal extrusion process. The PLA/BC extruded films were then foamed in a supercritical CO_2 batch foaming process and the effects of BC properties such as surface chemistry, shape, surface area and porosity on the PLA foaming process were examined. This work shows that BC can act as stabilizing agent as well as nucleating agent for foaming applications. However, the influence of BC on the final properties of PLA foam is dependent on BC physical properties such as size and porosity that are eventually related to the BC source as well as BC production conditions.

2. Experimental section

2.1. Materials

Since CO2 solubility is restricted to amorphous zones [21–25], we chose to perform all of the foaming experiments with amorphous PLA (polylactide) resin 4060D with $_{\rm D}$ -isomer content of 12% (Jumplast) and molecular weight ($M_{\rm w}$) of 113,600 g/mole. Differential scanning calorimetry (DSC) and thermogravimetric analysis (TGA) characterization of the neat PLA show amorphous polymer with glass transition temperature ($T_{\rm g}$) at 58 °C show no weight loss up to 310 °C, as presented in Supporting Information 1.

Biochar (BC) samples derived from sludge (SLG), pistachio shells (PST) and green waste (GW) were kindly provided by Bioforcetech. The biochar particles were ground and subsequently ball milled for 20 min to $<5\mu$ m size. BC particles were characterized with scanning electron microscopy (SEM) and Fourier transform infrared spectroscopy (FTIR). Surface area and pore size distribution were calculated by BET and BJH theories, respectively.

2.2. Foaming process

PLA foams were prepared by the two-step procedure described in Fig. 1. In the first step, PLA resins were coated with 1 mL mineral oil and then blended with 0.25, 0.5 and 1 g of BC, so that the total weight of PLA and the BC was 100 g. The BC-coated resins were then extruded through a 3/4 inch single-screw, (L/D ratio 25:1, compression ratio 3:1, C.W. Brabender). The extruder's four independent temperature zones were set to 170, 180, 180 and 170 °C. A 2-inch horizontal flex-lip ribbon die was set to 0.9 mm in thickness.

In the second step, PLA composites were cut into rectangular shapes of $10 \times 15 \times 0.9$ mm, inserted into a high-pressure vessel, and then saturated with supercritical CO₂. Soaking temperature of 40 °C was selected to enable optimal solubility of CO₂ in the PLA [19]. The reaction vessel

was depressurized for 60–90 second to promote gas bubble nucleation and cell growth. Various saturation pressures (100, 130, 180, 215, 280 and 330 bar) and soaking times (5,10, 15, 20 and 30 min) were studied to optimize the foaming process.

2.3. SEM/Foam characterization

Samples obtained by the method described above were cryofractured to expose the cellular morphology. Samples were sputter-coated with Au60Pd40 alloy using a Gressington 108Auto sputter coater operated at 20 mA for 90 s to completely coat the porous structure, then imaged using a scanning electron microscope (SEM, FEI XL30 Sirion with FEG source). ImageJ software (NIH) was used to analyze the cells to provide the number of cells, n; sampling area, A; and cell area. For each foam composition, cells were counted within a cross-sectional sampling area of around 4 mm² that included the top and bottom edges. The cell density, n_b, was calculated using Eqs. (1) and 2 as follows:

$$n_b = \left(\frac{n}{A}\right)^{\frac{3}{2}} E \tag{1}$$

The exponent is for the conversion from an area to volume basis. The expansion ratio, E, is determined by

$$E = \frac{\rho_u}{\rho_f} \tag{2}$$

Bulk densities of foam samples, ρ_f , and unfoamed samples, ρ_u , are measured using the water displacement method. The expansion ratio of the composite foams was determined in relation to the unfoamed bulk density of PLA. Approximating the cells as circles, the cell size was determined from the measured cell area. This method yields an average diameter of a given cell and not its maximum dimension. Two representative SEM images were used for each cell density, expansion ratio and cell size measurements.

3. Results

3.1. Optimization of foaming conditions

The PLA batch foaming process using supercritical ${\rm CO}_2$ is affected by many parameters including soaking pressure, time, pressure drop and temperatures [5,20]. These factors govern CO2 solubility and diffusion rate and, therefore, the foamability of PLA. Determination of solubility of CO2 in PLA is important because when gas encounters polymer under a high-pressure condition, it impregnates the polymer and then the polymer starts to swell. The amount of swelling depends on how much CO2 dissolves in the polymer. It also depends on the polymer's molecular configuration and architecture [5]. There is a significant body of literature on the solubility of CO2 in PLA. Oliveira et al. reported that the presence of PLA crystallites reduces CO2 solubility and, therefore, CO2 solubility in PLA will be higher in the amorphous phase [19]. Based on these studies, we optimized the soaking time and pressure conditions for neat PLA in our batch foaming system (Fig. 1B). A relatively low foaming temperature of 40 °C was chosen to perform all the experiments to enable optimal solubility of CO₂ in the PLA [19]. In addition, since below the melting point the solubility is restricted to amorphous zones [21-25], we chose to perform all of the foaming experiments with amorphous PLA.

The influence of soaking pressure on the foam quality is presented in Supporting Information 2 and summarized in Fig. 2. Pressures from 100 to 330 bars result in up to a 6-fold time increase in expansion ratios (Fig. 2A). However, the expansion ratio decreases with soaking pressure and levels off at 215 bars. Aionicesei et al. studied the solubility of supercritical CO₂ in PLA over similar temperature range to our experimental setup (35–50 °C) [26]. They found that CO₂ solubility in PLA reaches a certain plateau in pressure values of above 230 bars in which the solubility kept between 37 and 43%. Therefore, exceeding maximum gas concentration in the polymer will not necessarily affect foam

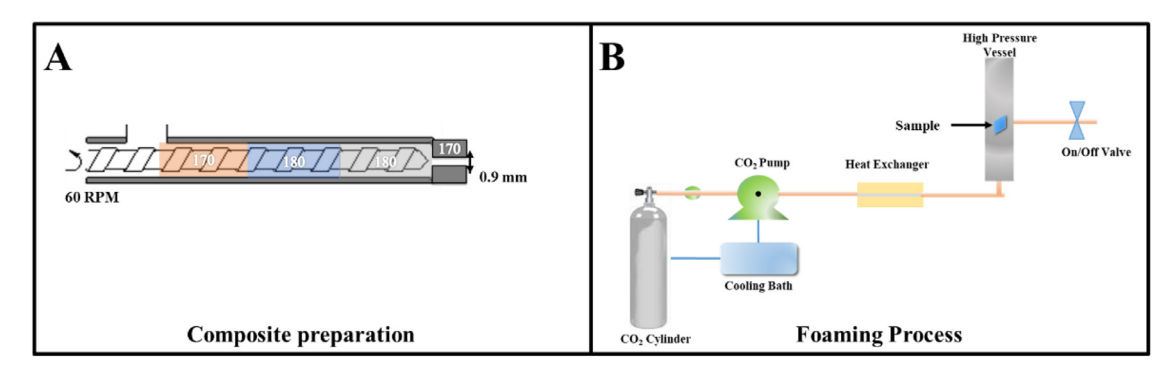


Fig. 1. A sketch describing the composite preparation (A) and foaming process (B) of PLA foam composites with biochar.

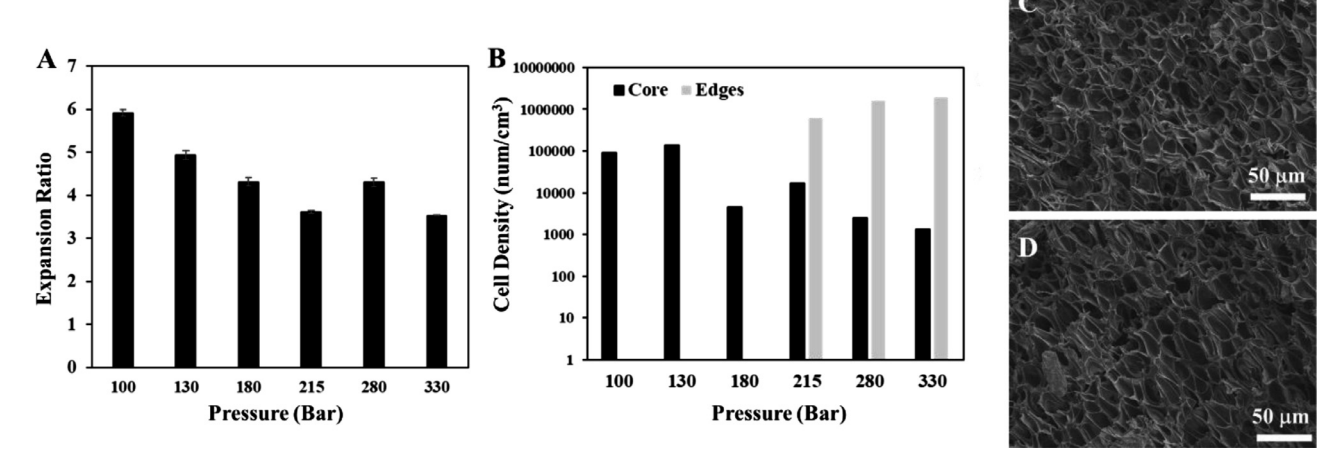


Fig. 2. Expansion ratio (A) and cell densities(B) of PLA foams soaked in 100, 130, 180, 215, 280 and 330 bars for 5 min. (B) Cross sectional 280 and 330 bar edges are presented in the SEM images C and D, respectively.

expansion. According to Muatana et al. cell nucleation and cell growth are competing processes for gas consumption during foaming CO_2 [27]. Therefore, we would expect to see a reduction in foam expansion with cell nucleation if the system has not reached equilibrium. SEM images that are presented in Supporting Information 2 show cell nucleation in PLA margins from 215 bars and unfoamed regions in the PLA cores suggesting CO_2 molecules have not completely diffused into the polymer and that the system has not reached equilibrium.

As expected, we observe a correlation between soaking pressure and CO_2 bubble nucleation. Cell nucleation during foaming is influenced by a polymer's interfacial tension, which decreases with pressure. When the saturation process is stopped before equilibrium, a concentration gradient across the sample leads to a wider distribution of cell sizes across the thickness of the final foamed sample [20].

The influence of saturation time on foam properties is presented in Supporting Information 3 and is summarized in Fig. 3. An increase in saturation time from 5 to 20 min resulted in a decrease in mean pore size from 117 to 11 μ m and increased cell density up to 4 orders of magnitude (Supporting Information 3). As expected, saturation time affects the cell size and morphology and thus the number of CO_2 molecules that have diffused into the PLA [5,20].

3.2. BC effect on PLA

3.2.1. Characterization of the BC particles

SEM images of the various BC particles (Fig. 4A-C) show particles with sharp edges and with no specific geometries. Surface morphology for all BC types is quite similar and is characterized by a relatively

smooth surface with no microporous surface that has typically been reported in the literature [28]. This is linked to the shear forces that the particles are subjected to during the ball milling process. The SEM images also reveal many finer BC particles with mean sizes less than 50 nm that are aggregated into larger bulk particles of 1–5 μm . The mean size of the particles is 0.91, 1.34 and 1.27 μm for SLG, PST and GW, respectively (Fig. 4D-F). However, all the particles are characterized by a very wide size distribution ranging from 0.15 to 5 μm . BET specific surface area measurements are 42, 126 and 188 m^2/g for the BC derived from SLG, PST and GW, respectively.

FTIR analysis was performed to further analyze the functional groups on the surfaces of the various BC particles. Understanding the surface chemical properties could help us anticipate the dispersibility of the BC particles. FTIR analysis of the BC particles (Fig. 3G-I) indicates that the BC particles from the different sources vary in their chemical group composition. SLG (Fig. 3G) particles are characterized with a band of approximately 1620 cm⁻¹, which usually represents C = O carbonyl groups [29]. The bands for aliphatic structures, including CH₃ and CH₂ groups, appear at 1430 cm⁻¹. The broad band from approximately 3000-3400 cm⁻¹ suggests large amounts of free and associated hydroxyl groups and structural hydroxyl groups (-COOH and -COH). Further evidence of OH stretches also appears with an intense peak at 1050 cm⁻¹. We assume that BC containing OH groups possess amphiphilic properties that can potentially interact with both hydrophilic and hydrophobic moieties in PLA through hydrogen bond interactions with the PLA ester linkage and therefore lead to improved dispersibility in the polymer.

Pistachio shells mainly contain cellulose content that provides strength and organization to the shell, and fats to dissolve nutrients and

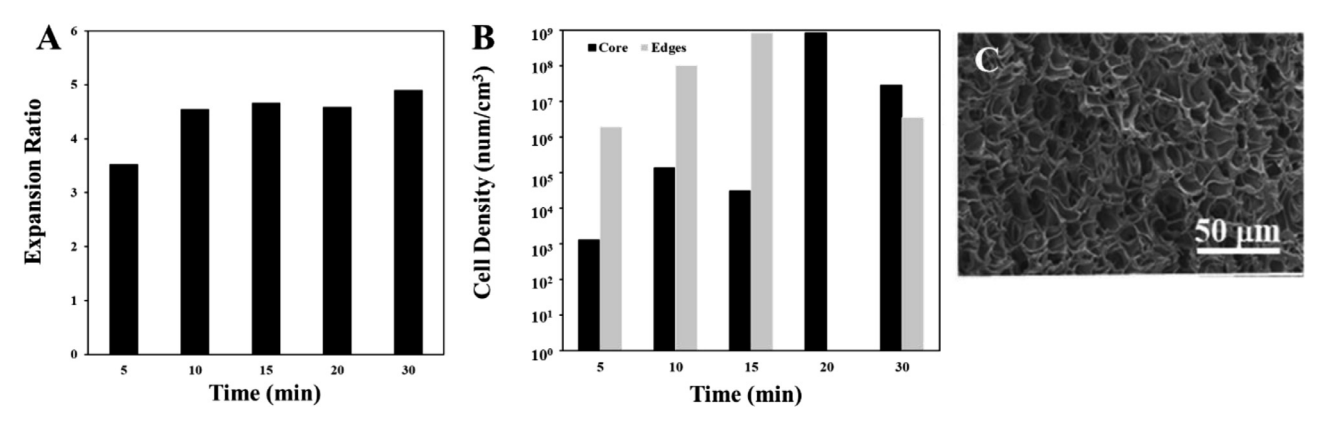


Fig. 3. Expansion ratio (A) and cell densities (B) of PLA foams soaked for 5, 10, 15, 20 and 30 min at 330 bar. (C) SEM image of PLA soaked for 20 min at 330 bar.

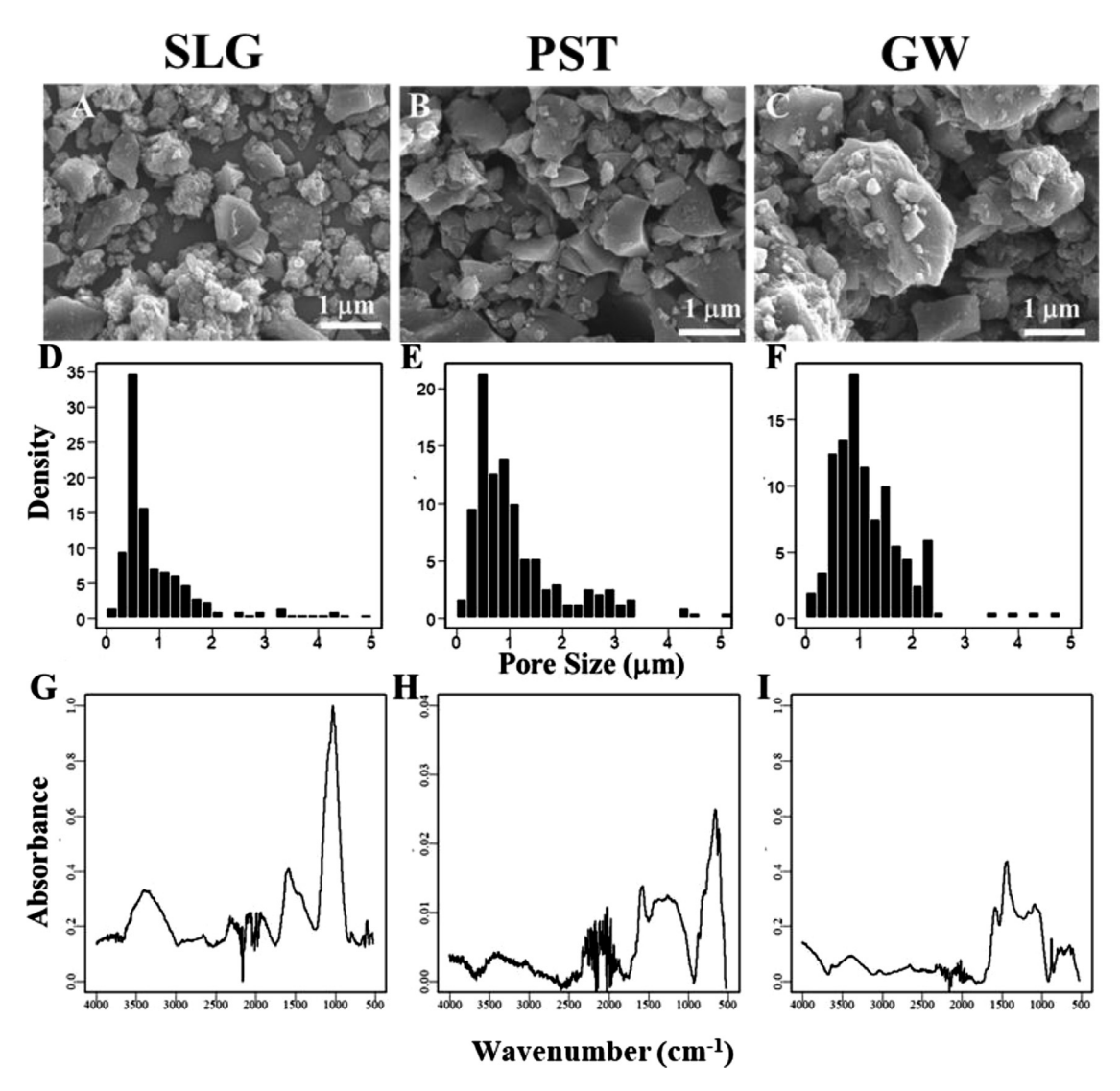


Fig. 4. SEM images (A-C), particle size distribution (D-F) and FTIR spectra (G-I) of the BC particles derived from SLG, PST and GW.

vitamins necessary for plant growth [30]. Previous studies showed that pyrolyzing pistachio shell showed cellulose groups as well as inorganic minerals such as kalicinite (KHCO₃) and halite (NaCl) [30]. The chemical nature of PST biochar depends on the pyrolysis temperature [30]. In our case, PST particles may be characterized by characteristic peaks of the aromatic C = O ring stretches that appear at 1500–1430 cm⁻¹.

The wide band at 1000–1385 cm⁻¹ is attributed to C = H vibration in alkanes and alkyl groups [30].

Like PST, GW is also characterized with lignocellulosic derived components in its FTIR spectrum (Fig. 3I). GW particles are characterized with a wide band at $1000-1420~{\rm cm}^{-1}$ that are attributed to C=H vibration in alkanes and alkyl groups. In addition, we observe a strong band

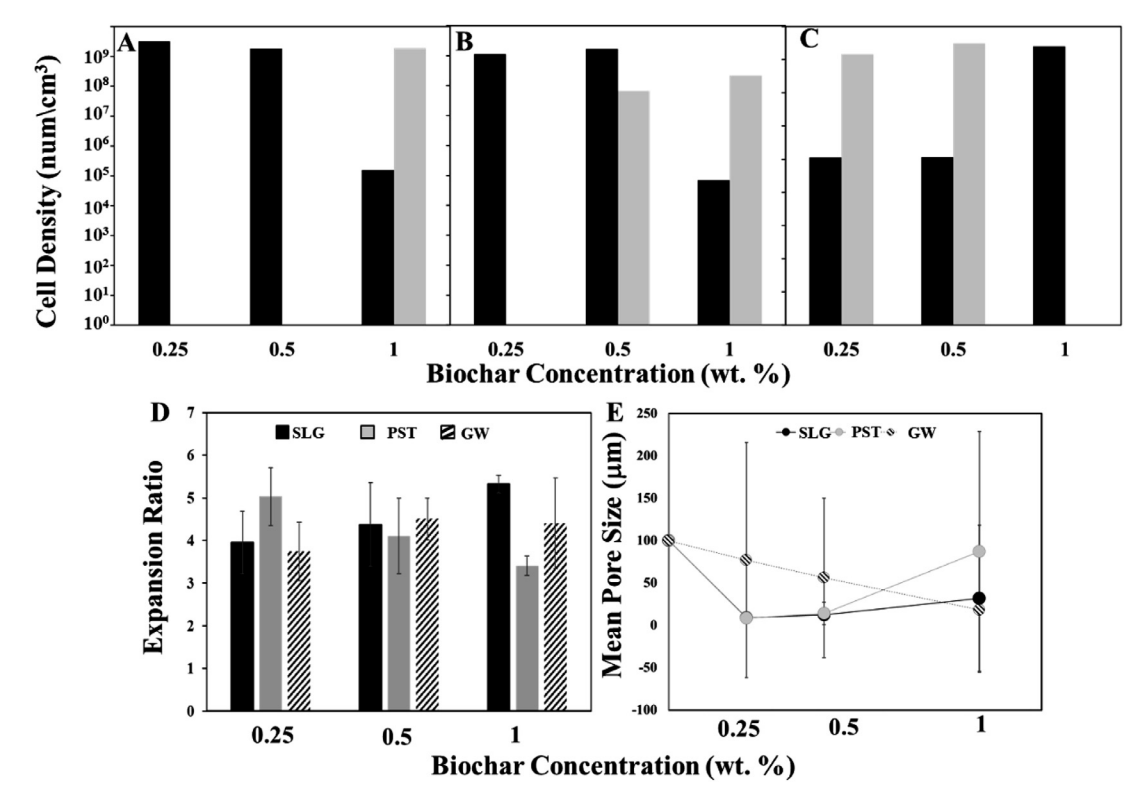


Fig. 5. Summary of PLA/BC foam properties: Cell densities of PLA foams with BC derived from SLG (A), PST (B) and GW (C), expansion ratio of PLA/BC foams (D), and mean pore size of the various PLA/BC foams (E).

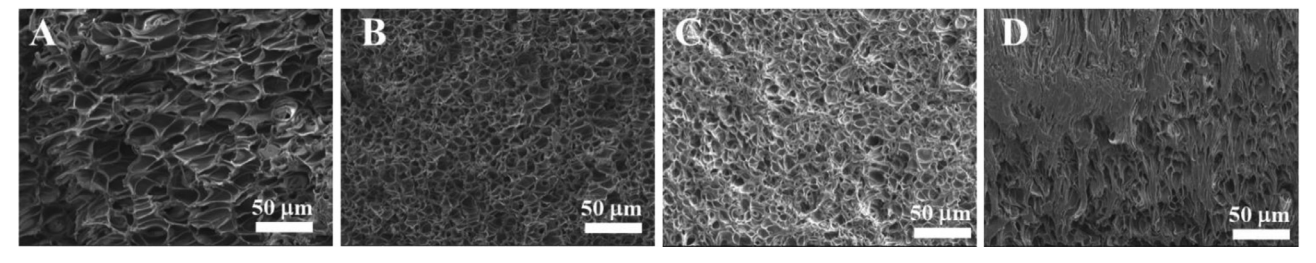


Fig. 6. Comparative SEM cross sectional images of neat PLA (A) and PLA with 0.25% BC from SLG (B), PST (C) and GW (D).

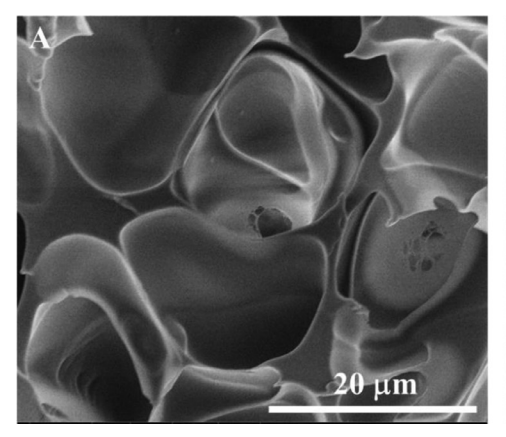
peaking at 1480 cm^{-1} that is attributed to C_6 ring modes, providing good evidence for the presence of aromatic structures [31].

3.2.2. BC effect on PLA foaming properties

The BC effect on the PLA foaming process was intentionally studied at 330 bars and 40 °C and so saturation time of 15 min was selected to show that BC addition can improve PLA final foam morphology. Analysis of the various PLA/BC foams is summarized in Figs. 5 and presented in Supporting Information 4 and 5. Cell density of the PLA/BC composite foams was found to be dependent on BC concentration and source. At low concentration (0.25%) PLA/BC shows homogenous cell density of 10⁹ cells/cm³ with up to 4 times increase in cell density and 10 time decrease in pore size compared to neat PLA (Fig. 5A-C and Fig. 3B). However, an increase in BC content resulted in a non-homogeneous cell density with low cell density regions and did not improve cell homogeneity. According to Lee et al., in most foaming cases of polymer/particle composites, the observed cell density is much lower than the potential particle density, implying that either particles are not effective nucleating agents or that their effect has been compromised due to poor dispersion [11,32]. For example, in previous studies with PLA/clay composites, exfoliated and intercalated clay platelets simultaneously exist, while the former dominate in low clay loadings [33]. Exfoliated structures (welldispersed in our case) present a higher number of potential nucleation sites and, thus, result in porous materials with higher cell density. Therefore, the increase in non-homogenous regions with the increase of BC content in PLA foams is attributed to an increased number of BC aggregates within PLA, as will be elaborated in detail in the Discussion section.

The effect of BC source on the foam cell morphology of PLA is presented in Fig. 6. Comparison of the cell morphology at low BC loading (0.25%) shows that the BC derived from different sources has different effects on the PLA cell morphology. We discovered that the neat PLA foam exhibits distorted cell shapes with diagonally aligned cells. PLA has inherently weak melt strength that negatively affects cell wall stability during foam expansion [34]. In addition to PLA's inherently low melt strength, supercritical $\rm CO_2$ acts as a plasticizer to PLA [34]. When a plasticizer is added to a polymer, it increases the polymer workability and flexibility. However, plasticizers also tend to lower the melt viscosity, the glass transition temperature and the elastic modulus. Li et al. demonstrated that the plasticization effect of dissolved $\rm CO_2$ gas reduced the viscosity of the PLA/gas mixture [35].

The fact that BC of various sources induced different cell morphologies (Fig. 6B-D) can be attributed to the differences in size distribution, dispersibilities and surface chemistries of the particles. The cell shapes



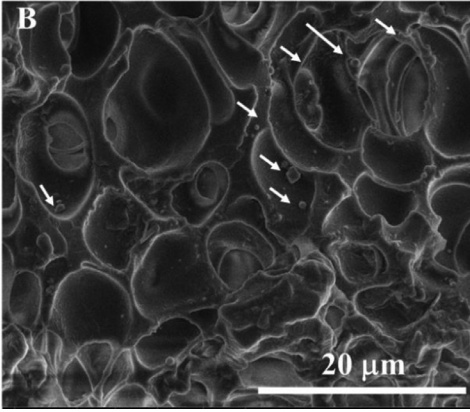


Fig. 7. Cross sectional SEM images of neat PLA and PLA with 0.25 wt% BC.

of the PLA/SLG and PLA/PST foams were approximate elliptical, uniform shapes, in case of PLA/GW we observed smeared cell morphologies and poor foaming structures with relatively high density. We propose that the differences between the various cell structures are related to differences in the dispersibilities and size distributions of the various BC within the PLA. Yang et al. suggested that the difference in the dispersibility of the particles along the polymer affect cell stretching during expansion and thereby the final cell morphology [36]. In the stretching stage, foam cells reduce stress concentrations between cells because of the large contact areas, resulting in a uniform deformation in the stretching direction. Neighboring cell walls begin to touch each other, and the foams can undergo plastic deformation so that uniform variations in stress are achieved during the stretching process. In the case of aggregates or large particles, the local stress variation around the cell walls leads to cell wall fracture with a decrease in tensile strength.

4. Discussion: BC as nucleating agents for PLA

Nucleation of bubbles can result from two mechanisms: homogeneous or heterogeneous. Homogeneous nucleation occurs when gas molecules dissolved in a homogeneous polymer diffuse together for a long enough period to produce a stable bubble nucleus [37]. Heterogeneous nucleation occurs when a bubble forms at an interface between two phases such as a polymer and an additive [37]. Addition of a solid surface to the polymer gas mixture affects the heterogeneous gas bubble nucleation density by lowering the free energy associated with bubble formation. The rate of heterogeneous nucleation, N, is given by Eq. (3) [37].

$$N = C_1 f \ e^{\left(\frac{-\Delta G_{shet}}{kT}\right)} \tag{3}$$

 C_1 is the concentration of the heterogenous nucleation sites, f is the frequency factor of gas molecules joining the nucleus, k and T are Boltzmann constant and temperature, respectively. $\Delta G_{^{\circ} \rm het}$ is the Gibbs free energy that is also dependent on the contact angle between the nucleating particle to the gas and the curvature of the particle surface. Based on Eq. (3), it is clear that particle properties such as surface chemistry and morphology could determine the likelihood of bubble formation during the foaming process.

In this work, we observed that BC derived from different sources induce different foam morphologies that vary in their foam cell density and cell structures. The different potential actions of a BC nucleating agent raise the question as to what makes an ideal bubble nucleating agent. McClurg tried to answer this question based on an analysis of the thermodynamics and kinetics of coupled nucleation and growth [38]. He proposed that there were four main characteristics for an ideal foam nucleating agent: i) Nucleation on ideal nucleates is energetically and kinetically favorable relative to homogeneous nucleation; ii) Ideal nucleating agents have uniform geometry and surface properties; iii) Nucle-

ating agents are easily dispersed and iv) Nucleating agents are plentiful enough to overwhelm the contributions of homogeneous and unintentional heterogeneous nucleation. In this discussion, we will analyze the likelihood of BC acting as a bubble nucleating agent for PLA based on McClurg's four criteria.

First, BC addition resulted in a PLA with cell density higher than for neat PLA (Fig. 3 and Fig. 5). Pore size analysis indicates that BC addition reduced mean pore size from $\sim\!100~\mu\mathrm{m}$ to less than $10~\mu\mathrm{m}$ (Fig. 5E). Previous studies also showed pore size reduction in PLA with the addition of nucleating agents [5,39,40]. SEM images in Fig. 7 present a comparison between the neat PLA cell structure and PLA/ w 0.25 wt% BC, thus providing further evidence that BC indeed induces PLA foam densification with smaller pore size foams and with BC particles. In addition, we can clearly observe BC particles on PLA cell walls suggesting BC particles are participating in cell formation (Fig. 7B, white arrows).

Comparison of the properties of various BC particles (Fig. 4) shows that BC derived from different sources differ in their size, surface area, porosity and chemistries. These factors determine the dispersibility of the particles within the polymer. In previous work with poly ε caprolactone, several nanoparticles of different geometries and dimensions, such as titanium dioxide, alumina powders, exfoliated and intercalated clays, as well as carbon nanotubes have been compared. Foam densities and morphologies, in terms of number of cells per initial unit volume, were found to depend on particle geometry and surface properties [41]. The BC particles are characterized with non-defined geometry and a wide size distribution, which can potentially reduce their dispersibility in PLA. Polarized optical microscopy (POM) images presented in Fig. 8 show a qualitive comparison between the PLA/BC films, suggesting that BC derived from SLG has better dispersibility in PLA due to the particles' chemical composition, smaller mean size and narrower size distribution.

We anticipated the we would observe a denser cell morphology with GW (188 m²/g) and PST (126 m²/g) compared to SLG (42 m²/g) due to a larger surface area and therefore potentially larger nucleation sites, yet we found the opposite trend. This result could also be related to the narrower size distribution of the BC derived from the SLG in comparison to GW and PST (Fig. 5D-F, Fig. 8). Another explanation could be related to the pore size distribution analysis of the BC particles. The pore size distribution of BC particles (Fig. 9) derived from SLG is characterized by a larger volume of mesopores structures in comparison to GW and PST. The mesopore structure in BC particles derived from SLG presents a larger number of bubble nucleation sites along the particle. Leung et al. demonstrated that the surface geometry of a heterogeneous nucleating site is a critical factor governing the free energy barrier to nucleating a bubble heterogeneously [42]. They found that nucleating agents with many crevices of small semi-conical angles lead to higher quality polymer foams, with a high cell density, a smaller cell size and narrower cell size distribution [42].



Fig. 8. POM images of extruded PLA films with 0.25 wt% BC derived from SLG (A), GW (B) and PST (C).

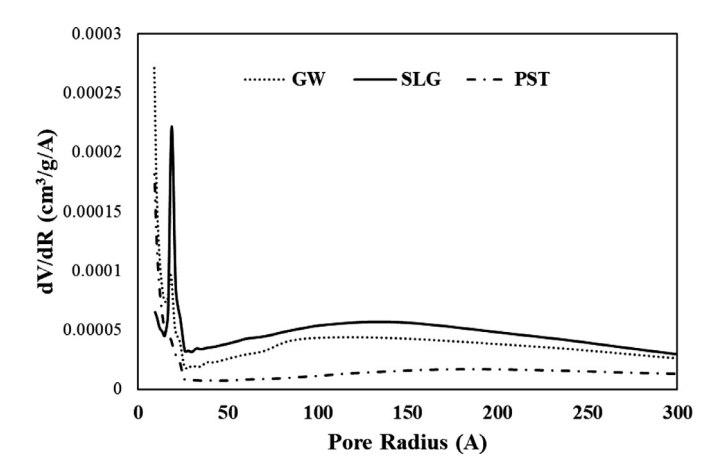


Fig. 9. Pore volume versus pore radius of the various BC particles, calculated according to the BJH method, as described in the experimental part.

Conclusions

In this work, we studied the ability of BC to assist in PLA foaming. Our goal was to fabricate PLA foams with similar or higher cell densities as expanded poly styrene foams (cell densities of $10^9 - 10^{12}$). We showed that BC is an effective class of nucleating agents that can increase PLA cell density up to four orders of magnitude with almost ten-fold decrease in mean pore size. This study reveals the potential of BC for foaming applications. BC are bioderived, cost-effective fillers that can act as nucleating agents in producing fully biodegradable PLA foams. Also, BC particles are relatively hydrophobic and therefore more easily dispersed in PLA in comparison to other fillers such as nanocrystalline cellulose or SiO_2 . Adversely, working with BC as additive fillers requires sieving and size reduction of the particles. In addition, particle effectiveness can vary depending on source and/or production method.

Declaration of Competing Interest

The authors declare that they have no known competing financial interests or personal relationships that could have appeared to influence the work reported in this paper.

Acknowledgments

This work is supported by the National Science Foundation, Grant CMMI-1727836. Any opinion, findings, and conclusions or recommendations expressed in this material are those of the authors and do not necessarily reflect the views of the National Science Foundation. Part of this work was performed at the Stanford Nano Shared Facilities (SNSF), supported by the National Science Foundation under award ECCS-1542152. The authors would also like to thank Dario Presezzi and Bioforcetech.

Supplementary materials

Supplementary material associated with this article can be found, in the online version, at doi:10.1016/j.apsadv.2021.100059.

References

- [1] T.P. Haider, C. Völker, J. Kramm, K. Landfester, F.R. Wurm, Plastics of the future? The impact of biodegradable polymers on the environment and on society, Angew. Chem. - Int. Ed. 58 (2019) 50–62, doi:10.1002/anie.201805766.
- [2] Y. Tokiwa, B.P. Calabia, Biodegradability and biodegradation of poly(lactide), Appl. Microbiol. Biotechnol. 72 (2006) 244–251, doi:10.1007/s00253-006-0488-1.
- [3] K. Madhavan Nampoothiri, N.R. Nair, R.P. John, An overview of the recent developments in polylactide (PLA) research, Bioresour. Technol. 101 (2010) 8493–8501, doi:10.1016/j.biortech.2010.05.092.
- [4] R. Auras, B. Harte, S. Selke, An overview of polylactides as packaging materials, (2004) 835–864. doi:10.1002/mabi.200400043.
- [5] M. Nofar, C.B. Park, Poly (lactic acid) foaming, Prog. Polym. Sci. 39 (2014) 1721– 1741, doi:10.1016/j.progpolymsci.2014.04.001.
- [6] L. Lim, R. Auras, M. Rubino, Processing technologies for poly (lactic acid), Prog. Polym. Sci. 33 (2008) 820–852, doi:10.1016/j.progpolymsci.2008.05.004.
- [7] F. Carrasco, P. Pagès, J. Gámez-pérez, O.O. Santana, M.L. Maspoch, Processing of poly (lactic acid): characterization of chemical structure, thermal stability and mechanical properties, Polym. Degrad. Stab. 95 (2010) 116–125, doi:10.1016/j.polymdegradstab.2009.11.045.
- [8] M.C. Gupta, V. Deshmukh, Thermal oxidative degradation of poly-lactic acid, Colloid Polym. Sci. 517 (1982) 514–517.
- [9] S.J. De Jong, E.R. Arias, D.T.S. Rijkers, C.F. Van Nostrum, New insights into the hydrolytic degradation of poly(lactic acid): participation of the alcohol terminus, Polymer (Guildf) 42 (2001) 2795–2802.
- [10] Y.M. Corre, A. Maazouz, J. Duchet, J. Reignier, Batch foaming of chain extended PLA with supercritical CO₂: influence of the rheological properties and the process parameters on the cellular structure, J. Supercrit. Fluids. 58 (2011) 177–188, doi:10.1016/j.supflu.2011.03.006.
- [11] J.L. Lee, C. Zeng, X. Cao, X. Han, J. Shen, X. Goujun, Polymer nanocomposites foams, Compos. Sci. Technol. 97 (2005) 2344–2363, doi:10.1016/j.compscitech.2005.06.016.
- [12] A. Rita, C. Duarte, V.E. Santo, A. Alves, S.S. Silva, J. Moreira-silva, T.H. Silva, A.P. Marques, R.A. Sousa, M.E. Gomes, J.F. Mano, R.L. Reis, Unleashing the potential of supercritical fluids for polymer processing in tissue engineering and regenerative medicine, J. Supercrit. Fluids. 79 (2013) 177–185, doi:10.1016/j.supflu.2013.01.004.
- [13] J. Dlouhá, L. Suryanegara, H. Yano, The role of cellulose nanofibres in supercritical foaming of polylactic acid and their effect on the foam morphology, Soft Matter 8 (2012) 8704–8713, doi:10.1039/c2sm25909e.
- [14] R. Liao, W. Yu, C. Zhou, Rheological control in foaming polymeric materials: I. Amorphous polymers, Polymer (Guildf). 51 (2010) 568–580, doi:10.1016/j.polymer.2009.11.063.
- [15] E. Richards, R. Rizvi, A. Chow, H. Naguib, Biodegradable composite foams of PLA and PHBV using subcritical CO₂, J. Polym. Environ. 16 (2008) 258–266, doi:10.1007/s10924-008-0110-y.
- [16] M. Murariu, A.-L. Dechief, R. Ramy-Ratiarison, Y. Paint, J.-M. Raquez, P. Dubois, Recent advances in production of poly(lactic acid) (PLA) nanocomposites: a versatile method to tune crystallization properties of PLA, Nanocomposites 1 (2015) 71–82, doi:10.1179/2055033214Y.0000000008.
- [17] A. Pei, Q. Zhou, L.A. Berglund, Functionalized cellulose nanocrystals as biobased nucleation agents in poly(I-lactide) (PLLA) - crystallization and mechanical property effects, Compos. Sci. Technol. 70 (2010) 815–821, doi:10.1016/j.compscitech.2010.01.018.
- [18] W.G. Zheng, Y.H. Lee, C.B. Park, Use of nanoparticles for improving the foaming behaviors of linear PP, J. Appl. Polym. Sci. 117 (2010) 2972–2979, doi:10.1002/app.
- [19] N.S. Oliveira, J. Dorgan, J.A.P. Coutinho, A. Ferreira, J.L. Daridon, I.M. Marrucho, Gas solubility of carbon dioxide in poly (lactic acid) at high pressures, J. Polym. Sci. Part B Polym. Phys. 44 (2005) 1010–1019, doi:10.1002/polb.20746.
- [20] S.K. Goel, E.J. Beckman, Generation of microcellular polymeric foams using supercritical carbon dioxide. I: effect of pressure and temperature on, Polym. Eng. Sci. 34 (1994) 1137–1147.

- [21] D.F. Baldwin, S. Minuro, S. Nam P, The role of gas dissolution and induced crystallization during microcellular polymer processing: a study of poly (ethylene terephthalate) and carbon dioxide systems. J. Eng. Mater. Technol. 117 (1995) 62–74.
- [22] X. Liao, A.V. Nawaby, P.S. Whitfield, Carbon dioxide-induced crystallization in poly(L-lactic acid) and its effect on foam morphologies, Polym. Int. 59 (2010) 1709– 1718, doi:10.1002/pi.2910.
- [23] Saeed Doroudiani, Chul B. Park, Mark T. Kortschot, Effect of the crystallinity and morphology on the microcellular foam structure of semicrystalline, Polym. Eng. Sci. (1996) 36, doi:10.1002/pen.10664.
- [24] S. Doroudiani, C.B. Park, M.T. Kortschot, Processing and characterization of microcellular foamed high-density polyethylene/isotactic polypropylene blends, Polym. Eng. Sci. 38 (1998) 1205–1215. doi:10.1002/pen.10289.
- [25] M. Sauceau, J. Fages, A. Common, C. Nikitine, E. Rodier, New challenges in polymer foaming: a review of extrusion processes assisted by supercritical carbon dioxide, Prog. Polym. Sci. 36 (2011) 749–766, doi:10.1016/j.progpolymsci.2010.12.004.
- [26] E. Aionicesei, M. Skerget, Measurement of CO₂ solubility and diffusivity in poly (L -lactide) and poly (D, L -lactide- co -glycolide) by magnetic suspension balance, J. Supercrit. Fluids. 47 (2008) 296–301, doi:10.1016/j.supflu.2008.07.011.
- [27] L.M. Matuana, C.A. Diaz, Study of cell nucleation in microcellular poly(lactic acid) foamed with supercritical CO₂ through a continuous-extrusion process, Ind. Eng. Chem. Res. 49 (2010) 2186–2193.
- [28] P. Baltr, E. Baltr, Biochar from pine and birch morphology and pore structure change by treatment in biofilter, Water Air Soil Pollut 226 (2015) 1–14, doi:10.1007/s11270-015-2295-8.
- [29] J. Jin, Y. Li, J. Zhang, S. Wu, Y. Cao, P. Liang, J. Zhang, M. Hung, M. Wang, S. Shan, P. Christie, Influence of pyrolysis temperature on properties and environmental safety of heavy metals in biochars derived from municipal sewage sludge, J. Hazard. Mater. 320 (2016) 417–426, doi:10.1016/j.jhazmat.2016.08.050.
- [30] K. Komnitsas, D. Zaharaki, I. Pyliotis, D. Vamvuka, G. Bartzas, Assessment of pistachio shell biochar quality and its potential for adsorption of heavy metals, Waste Biomas Valorization 5 (2015) 805–816.
- [31] W. Azlina, W. Abdul, K. Ghani, A. Mohd, R.T. Bachmann, Y.H. Taufiq-yap, U. Rashid, A.H. Al-muhtaseb, Biochar production from waste rubber-wood-sawdust and its potential use in C sequestration: chemical and physical characterization, Ind. Crop. Prod. 44 (2013) 18–24, doi:10.1016/j.indcrop.2012.10.017.

- [32] A. Tsimpliaraki, I. Tsivintzelis, S.I. Marras, I. Zuburtikudis, C. Panayiotou, The effect of surface chemistry and nanoclay loading on the microcellular structure of porous poly (D, L lactic acid) nanocomposites, J. Supercrit. Fluids. 57 (2011) 278–287, doi:10.1016/j.supflu.2011.03.010.
- [33] D. Wee, D.G. Seong, J.R. Youn, Processing of microcellular nanocomposite foams by using a supercritical fluid, Fibers Polym. 5 (2004) 160–169.
- [34] Q.I. Zhou, L.A. Berglund, Poly(lactic acid) science and technology: processing, properties, additives and applications, 2015.
- [35] D. Li, T. Liu, L. Zhao, X. Lian, W. Yuan, Foaming of poly (lactic acid) based on its nonisothermal crystallization behavior under compressed carbon dioxide, Ind. Eng. Chem. Res. (2011) 1997–2007, doi:10.1021/ie101723g.
- [36] C. Yang, M. Wang, S. Xing, Q. Zhao, M. Wang, G. Wu, A new promising nucleating agent for polymer foaming: effects of hollow molecular-sieve particles on polypropylene supercritical CO₂ microcellular foaming, RSC Adv 8 (2018) 20061–20067. doi:10.1039/c8ra03071e.
- [37] S.J. Colton, Nucleation of microcellular foam: theory and practice, Polym. Eng. Sci. 27 (1987) 500–503.
- [38] R.B. McClurg, Design criteria for ideal foam nucleating agents, Chem. Eng. Sci. 59 (2004) 5779–5786, doi:10.1016/j.ces.2004.06.025.
- [39] S.H. Mahmood, M. Keshtkar, C.B. Park, Determination of carbon dioxide solubility in polylactide acid with accurate PVT properties, J. Chem. Thermodyn. 70 (2014) 13–23, doi:10.1016/j.jct.2013.10.019.
- [40] T.R. Kuang, H.Y. Mi, D.J. Fu, X. Jing, B.Y. Chen, W.J. Mou, X.F. Peng, Fabrication of poly(lactic acid)/graphene oxide foams with highly oriented and elongated cell structure via unidirectional foaming using supercritical carbon dioxide, Ind. Eng. Chem. Res. 54 (2015) 758–768, doi:10.1021/ie503434q.
- [41] C. Marrazzo, E. Di Maio, S. Iannace, Conventional and nanometric nucleating agents in poly (e-caprolactone) foaming: crystals vs. bubbles nucleation, Polym. Eng. Sci. 10 (2008) 336–344, doi:10.1002/pen.
- [42] S.N. Leung, A. Wong, C.B. Park, J.H. Zong, Ideal surface geometries of nucleating agents to enhance cell nucleation in polymeric foaming processes, J. Appl. Polym. Sci. 108 (2008) 3997–4003, doi:10.1002/app.